A Split-Based Approach to Unsupervised Change Detection in Large-Size Multitemporal Images: Application to Tsunami-Damage Assessment

Francesca Bovolo, *Member, IEEE*, and Lorenzo Bruzzone, *Senior Member, IEEE*

***Abstract*—This paper presents a split-based approach (SBA) to automatic and unsupervised change detection in large-size multitemporal remote-sensing images. Unlike standard methods that are presented in the literature, the proposed approach can detect in a consistent and reliable way changes in images of large size also when the extension of the changed area is small (and, therefore, the prior probability of the class of changed pixels is very small). The method is based on the following: 1) a split of the large-size image into subimages; 2) an adaptive analysis of each subimage; and 3) an automatic split-based threshold-selection procedure. This general approach is used for defining a system for damage assessment in multitemporal synthetic aperture radar (SAR) images. The proposed system has been developed to properly identify different levels of damages that are induced by tsunamis along coastal areas. Experimental results that are obtained on multitemporal RADARSAT-1 SAR images of the Sumatra Island, Indonesia, confirm the effectiveness of both the proposed SBA and the presented system for tsunami-damage assessment.**

***Index Terms*—Change detection, damage assessment, disaster monitoring, image analysis, multitemporal images, remote sensing, synthetic aperture radar (SAR) images, tsunami, unsupervised techniques.**

I. Introduction

In RECENT years, the frequency of natural disasters has shown rapid increase [1].[1] Examples of this trend are related to floods, earthquakes, avalanches, hurricanes, forest fires, and tsunamis that recently occurred. These dramatic events increased the interest of politic and scientific communities in the definition of methodologies that are capable to prevent them, mitigate their effects, and perform fast and accurate damage assessment. Satellite remote-sensing images that are acquired on the same area at different times are a valuable tool for addressing the aforementioned problems. The information that is present in these data can be useful for extracting important indications for risk assessment, emergency management, and damage inventory. In this paper, we focus the attention on the problem of damage inventory.

In order to perform effective damage inventory, it is important to develop proper change-detection techniques for the automatic analysis of multitemporal remote-sensing images. In the literature, many techniques have been proposed for change detection in both optical and synthetic aperture radar (SAR) remote-sensing data [2]–[21]. Often, changes are identified by comparing pixel by pixel two images that are acquired on the same geographical area at two different times. The comparison can be carried out according to a difference operator (this is the typical case of multispectral images) or a ratio/log-ratio operator (as usually done in a SAR image), as well as with more complex strategies based on context-sensitive dissimilarity measures that are computed between statistical distributions [14]. The resulting difference/ratio image is then analyzed according to either automatic thresholding algorithms [6]–[10], [19], [20] or complex context-sensitive [5], [21] and multiscale algorithms [15] to generate the final change-detection map. For simplicity, let us focus the attention on thresholding algorithms, which are the most widely used in the applications (however, the discussion can be easily generalized to context-sensitive and multiscale procedures). Most of the thresholding algorithms derive automatically the change-detection map under the assumption that the prior probability of the class of changed pixels is sufficient to properly model this class with a significant statistical mode in the histogram of the difference/ratio image. However, as the aforementioned kinds of damages typically affect local portions of wide areas (e.g., regions or countries), a proper damage-assessment procedure requires the analysis of wide scenes and, thus, of large-size images. This results in a small value of the prior probability of the class of changed pixels, which may affect the capabilities of the thresholding techniques to detect a proper threshold value if working on the whole image.

In the image-processing literature, local adaptive thresholding techniques have been proposed for characterizing the local properties of images. In change-detection problems, these techniques compute a threshold value for each pixel neighborhood on the basis of local statistics and apply it to either the entire neighborhood or only the central pixel [16], [22]. As these methods result in many isolated change pixels and holes in the middle of connected change components, postprocessing steps are usually adopted for reducing noise in the final change-detection map and making it consistent with the hypothesis that changes are made up of a significant number of connected pixels [16]. Alternative approaches, which are mainly proposed for threshold-based classification of large-size images, perform an independent analysis of overlapping image blocks that results in

Manuscript received June 19, 2006; revised November 3, 2006. This work was supported by the Italian Ministry of Education, University and Research.

The authors are with the Department of Information and Communication Technologies, University of Trento, 38050 Trento, Italy (e-mail: lorenzo.bruzzone@ing.unitn.it).

Digital Object Identifier 10.1109/TGRS.2007.895835

[1]See also www.panda.org, www.climate.org, and www.ifrc.org.

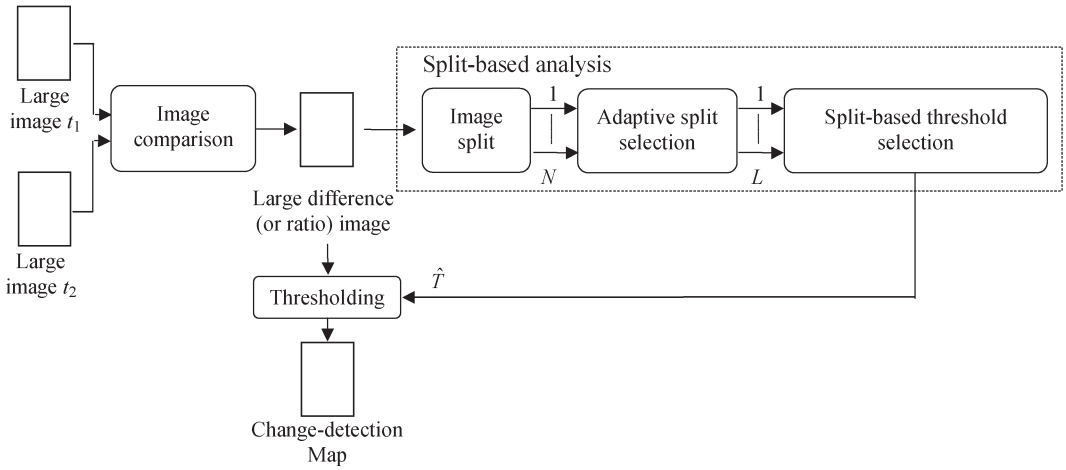

Fig. 1. Block scheme of the proposed SBA for change detection in large-size multitemporal images.

different threshold values for each considered region [23]–[25]. However, in remote-sensing change-detection problems, a pixel-based threshold selection in local neighborhoods or a simple split of a large-size image into several smaller subimages and a successive separate analysis and thresholding of each split can be critical because of three conditions: 1) The threshold values should be consistent in all subimages/blocks to obtain significant change-detection maps also from a quantitative viewpoint (a single threshold value should be used in the entire large-size image to obtain consistency with the radiometric properties of the data). 2) Possible threshold-selection errors on a split/block generate inaccurate change-detection results for that subimage. 3) Changes might not be present in some subimages (and several thresholding algorithms used in remote-sensing applications implicitly assume the presence of two distributions and are not able to detect situations of absence of changes).

In order to overcome the aforementioned problems, in this paper, we propose an unsupervised split-based approach (SBA) for change detection in large-size multitemporal images, which is suitable for handling both multispectral images that are acquired by passive sensors and SAR images that are acquired by active sensors. The proposed method automatically splits the computed difference (or ratio) image in a set of nonoverlapping subimages of user-defined size. Then, the subimages are sorted out according to their probability to contain a significant amount of changed pixels. Afterward, a subset of splits having high probability to contain changes is selected and analyzed. Under the assumption that these splits represent reliable observations of the same phenomenon of change, it is expected that the threshold-selection procedure is reliable on them, as they are characterized by the highest prior probabilities of the change class among all splits. In order to properly extract the change information by thresholding the whole scene, two different strategies can be used for combining information that is present in different subimages. The first strategy is based on an independent split analysis that consists in applying threshold selection separately to each split for deriving a set of threshold values (one for each subimage). Hence, simple combination techniques can be applied to the obtained set of thresholds to select a robust, unique, and consistent threshold value to be applied to the entire image. The second strategy exploits a joint split analysis that consists in applying thresholding to the joint distribution of pixels that is obtained by merging all the splits having high probability to contain changes.

The proposed general method is used for defining a system based on multitemporal SAR images for damage assessment in areas that are affected by a tsunami. The proposed system is tested on two images that are acquired by the SAR sensor of the RADARSAT-1 satellite over Sumatra Island, Indonesia, in April 1998 and in January 2005. Between the two acquisitions, a tsunami destroyed large parts of the coast. Experimental results show that the proposed technique produces accurate change-detection maps that are capable of identifying major damages that are caused by the tsunami on the coast.

This paper is organized into five sections. Section II describes the proposed general SBA for change detection in large-size multitemporal images. Section III presents a system for tsunami-damage assessment, which exploits the proposed SBA and multitemporal SAR images. Section IV reports experimental results that are obtained on multitemporal SAR images of the Sumatra Island. Finally, Section V draws the conclusions of this paper.

II. Proposed SBA for Change Detection in Large-Size Multitemporal Images

Let us consider two coregistered remote-sensing images $\mathbf{X}_1$ and $\mathbf{X}_2$, of size $P \cdot Q$, that are acquired over the same area at different times t_1 and t_2.[2] Let $\mathbf{\Omega} = \{\omega_n, \omega_c\}$ be the set of classes of unchanged and changed pixels to be identified. As shown in Fig. 1, the architecture of the proposed SBA is based on three main blocks aimed at the following: 1) image comparison; 2) split of the large-size image into N subimages and selection of the L $(L \leq N)$ splits having the highest probabilities to include changes; and 3) split-based threshold selection. In the following, these blocks are described in greater detail.

[2]In this paper, only the case of pairs of images is discussed. However, the proposed approach can be applied to a multitemporal sequence that is made up of more than two images by analyzing separately couples of images.

A. Image Comparison

The first step of the most widely used change-detection techniques that are presented in the literature is based on a pixel-by-pixel (or parcel-by-parcel [5]) comparison between the two considered images, which is carried out according to a proper operator [11]–[15], [17], [18].

When dealing with multispectral images, each spatial position in $\mathbf{X}_1$ and $\mathbf{X}_2$ can be represented by an n-dimensional vector, whose components are associated with the radiances that are measured in different spectral channels. The most widely used comparison operator with this kind of images is the difference that is applied to the n-dimensional feature vectors, which allows to consider in the change-detection process all the available spectral information. Generally, difference image $\mathbf{X}_D$ is computed as the magnitude of the difference vectors. This technique is known as change vector analysis [2], [6] and has been successfully used in many different application domains.

When dealing with SAR images, either the difference or the ratio operator can be used [9]–[13]. However, the difference operator leads to an image that has a statistical distribution that depends on both the relative change of backscattering between the two acquisition dates and the reference intensity value. This results in different statistical behaviors of changed pixels in image portions that show different absolute backscattering values. To avoid this problem, comparison in SAR images is typically carried out by a ratio operator, which reduces the multiplicative distortion effects of noise that are common to the two considered images due to speckle and makes the statistical distribution of the resulting image dependent only on the relative changes between the two acquisitions. Usually, the ratio image is expressed in a logarithmic scale to enhance low-intensity pixels [11]–[13], [15] (and to obtain a more symmetrical distribution of the classes of changed and unchanged pixels), resulting in the log-ratio image $\mathbf{X}_{LR}$.

Instead of comparing the values of each single pixel, one may compare the probability density functions (pdfs) that are evaluated in a neighborhood of the considered spatial position in the two multitemporal images, according to proper dissimilarity measures [14]. As an alternative, it is possible to derive multitemporal parcels [5] and apply the comparison at a parcel level (after the extraction of proper parcel-based features).

B. Image Split and Adaptive Split Selection

Let $\mathbf{X}_C$ be the image (of size $P \cdot Q$) that is obtained after comparison of multitemporal data. The most widely used unsupervised approach for change detection is to apply a threshold-selection algorithm to $\mathbf{X}_C$ and to generate the change-detection map accordingly to the derived threshold value. Usually, the threshold-selection algorithms assume that the class of changed pixels can be associated with a reliable statistical mode in the histogram of $\mathbf{X}_C$. This assumption is critical in large-size images, as typically the phenomenon that involves changes only affects a small portion of the scene. This results in a very small prior probability of the class of change and, thus, in an almost indistinct mode in the histogram, which may involve a failure of the threshold-selection algorithms. In order to overcome this problem, we propose to split the image $\mathbf{X}_C$ in a set of subimages. The image-splitting procedure takes as input the large-size image $\mathbf{X}_C$ and subdivides it into a set of N subimages $\mathbf{X}_{C_i}$, $i = 1, \ldots, N$, of user-defined size $(p \cdot q)$ (see Fig. 2). The choice of the values of p and q depends on the geometric resolution of the sensor and on the expected extension of change that occurred in the investigated area. The basic requirement is that the amount of changes in a subset of splits should be statistically significant for making the threshold-selection procedure reliable and precise (empirically, we can assume that 10% of the changed pixels is sufficient for guaranteeing high accuracy with proper threshold-selection algorithms [18]). An estimation of the split size (and, thus, of N) can be obtained by relating the aforementioned concepts with the size of the whole image. According to the hypothesis that changed pixels have very small prior probability with respect to unchanged pixels, most of the generated subimages (splits) $\mathbf{X}_{C_i}$ have high probability to contain either no changes or a nonsignificant amount of changed pixels. We expect that only a few of them contain a number of changed pixels that are sufficient for characterizing this class in a statistically significant way. Under this realistic assumption, in most of the subimages, standard threshold-selection techniques may not identify proper threshold values because of two conditions: 1) Most of them implicitly assume the presence of changes; thus, when there are no changes, they identify meaningless threshold values. 2) They assume that the change class has a sufficiently high prior probability to yield a statistically significant mode in the histogram. In order to avoid such kind of problems, the set of subimages with the highest probability to contain changes is identified. This task is carried out by analyzing the global statistical behaviors of the computed subimages. Let P_{C_i} be the probability that the subimage $\mathbf{X}_{C_i}$ includes changed pixels. We reasonably expect that, when considering a difference (or ratio) operator in the comparison, P_{C_i} is a function of the standard deviation σ_i of subimage $\mathbf{X}_{C_i}$ (which is used as an index for changes in [16], [23], and [24]),[3] i.e.,

$$P_{C_i} = f(\sigma_i) \tag{1}$$

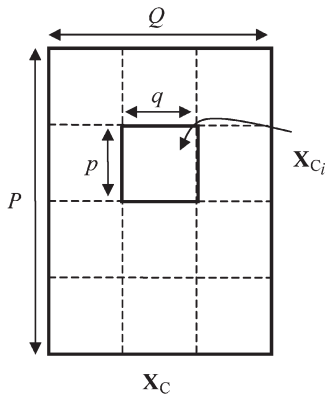

Fig. 2. Example of splitting a large image of size $P \cdot Q$ into N splits of size $p \cdot q$.

[3]An alternative measure to the standard deviation is the coefficient of variation, which becomes useful when the noise of subimages can be modeled as multiplicative or a residual multiplicative component is present in the splits [15].

where $f(.)$ is a monotonic function that increases by increasing the value of σ_i. According to this definition, irrespectively of the analytical form of $f(.)$, the set $\mathcal{P}_C$ of subimages that are ordered according to the probability of including changes can be derived as

$$\mathcal{P}_C = \{\mathbf{X}_{C_i} | \sigma_i \geq \sigma_{i+1}, i = 1, \ldots, N\}. \quad (2)$$

The desired set $\mathcal{P}'_C \subseteq \mathcal{P}_C$ of splits with the highest probabilities to contain changes is defined by selecting the first L elements of $\mathcal{P}_C$, i.e.,

$$\mathcal{P}'_C = \{\mathbf{X}_{C_1}, \mathbf{X}_{C_2}, \ldots, \mathbf{X}_{C_L} | \sigma_1 \geq \sigma_2 \geq \cdots \geq \sigma_L, L \leq N\}. \quad (3)$$

C. Split-Based Threshold Selection

Subimages in $\mathcal{P}'_C$ can be analyzed according to different strategies in order to identify a threshold value that is reliable for the whole large-size image and consistent with the radiometric properties of the data. Two main approaches can be distinguished: 1) an independent split analysis strategy based on the combination of reliable split-based threshold values and 2) a joint split analysis strategy based on the combination of splits distributions and threshold selection.

The independent split analysis strategy is based on a separate analysis of the L subimages that are included in $\mathcal{P}'_C$ and on a combination of decisions that are taken on each subimage. The first step of this approach is to compute a set $\mathcal{T} = \{T_1, \ldots, T_L\}$ of threshold values (one for each considered split in $\mathcal{P}'_C$) according to any of the thresholding procedures that are proposed in the literature (e.g., generalized Kittler and Illingworth (KI) algorithm [7], [9], [10] and generalized Expectation–Maximization-based algorithm [8], [17], [18]). In order to compute the final threshold value $\hat{T}$ to be applied to the whole image, different combination strategies can be adopted: 1) Compute the mean of the threshold values in $\mathcal{T}$ (Mean-SBA), and 2) compute the median of the threshold values in $\mathcal{T}$ (Med-SBA). The mean is the simplest mathematical operator that can be adopted for estimating threshold value $\hat{T}$. Although from a statistical point of view the mean operator produces a reliable result, it has the drawback that, in the presence of a few samples, it is slightly sensitive to outliers and may find an inconsistent threshold value if, for a few subimages in $\mathcal{P}'_C$, unreliable threshold values are computed. This may be a critical problem, as in real applications, it may happen that the threshold-selection algorithm does not provide reliable results on a split.[4] This problem can be overcome by adopting the median operator instead of the mean one.

The joint split analysis strategy to threshold selection is an alternative to the independent one. It performs simultaneous analysis of the selected splits (J-SBA) and then directly derives the final value of the decision threshold. The main idea that is exploited in this procedure is to jointly characterize the populations of changed and unchanged pixels using all the splits in $\mathcal{P}'_C$ and to apply threshold selection to this joint distribution. The first step of this procedure is to define a new random variable that is given by the union of the radiances of all the L selected subimages candidate to contain changes, i.e.,

$$\mathbf{X}'_C = \bigcup_{i=1}^{L} \mathbf{X}_{C_i}, \qquad \mathbf{X}_{C_i} \in \mathcal{P}'_C. \quad (4)$$

In this way, the distribution of $\mathbf{X}'_C$ properly represents the change-detection problems that are modeled in all the L splits, guaranteeing a reasonable prior probability for the class of changed pixels. Therefore, threshold value $\hat{T}$ can be derived by applying threshold selection to $\mathbf{X}'_C$. On the one hand, this allows one the selection of a reliable threshold value without any combination of the split-based threshold values. On the other hand, possible nonstationarity of the distributions of classes of changed and unchanged pixels in different splits may affect the reliability of the statistical models that are used for representing class distributions in thresholding algorithms. This may decrease the accuracy of the threshold-selection procedure.

Irrespectively of the threshold-selection strategy considered, the final change-detection map $\mathbf{X}_M$ is computed by applying the estimated threshold $\hat{T}$ to the large-size image $\mathbf{X}_C$.

III. Novel Split-Based System for Tsunami-Damage Assessment

In this section, the general technique that is presented previously for unsupervised change detection in large-size multitemporal images is exploited for designing an automatic system for tsunami-damage assessment in multitemporal SAR images. Additional blocks with respect to the base scheme of Fig. 1 are necessary to handle this complex problem. In the following, after proper problem description, we present the architecture of the proposed system.

A. Data Set and Problem Description

The problem of damage assessment after a tsunami was studied and addressed by using two intensity images that are acquired by the SAR sensor of the RADARSAT-1 satellite over the north part of the Sumatra Island, Indonesia. The available data have a pixel spacing of 25 m in both the azimuth and range directions. A tsunami strongly affected this area on December 26, 2004. After this date, different kinds of sensors acquired many images over the site that is interested by the natural disaster [26]. For this reason, it was possible to have an image acquired after a few days from the tsunami (January 2005). Unfortunately, the image in the archive that was acquired by RADARSAT-1 before December 2004 was taken on April 1998. The time distance between the two multitemporal images is due to the need, given the acquisition after the tsunami, to find in the archives an image before the tsunami event

[4]Even if robust threshold-selection procedures are used (i.e., procedures for which the probability to detect a wrong threshold value is very small if the prior probability of changed pixels is not too small), it may happen that an imprecise value is selected on a split.

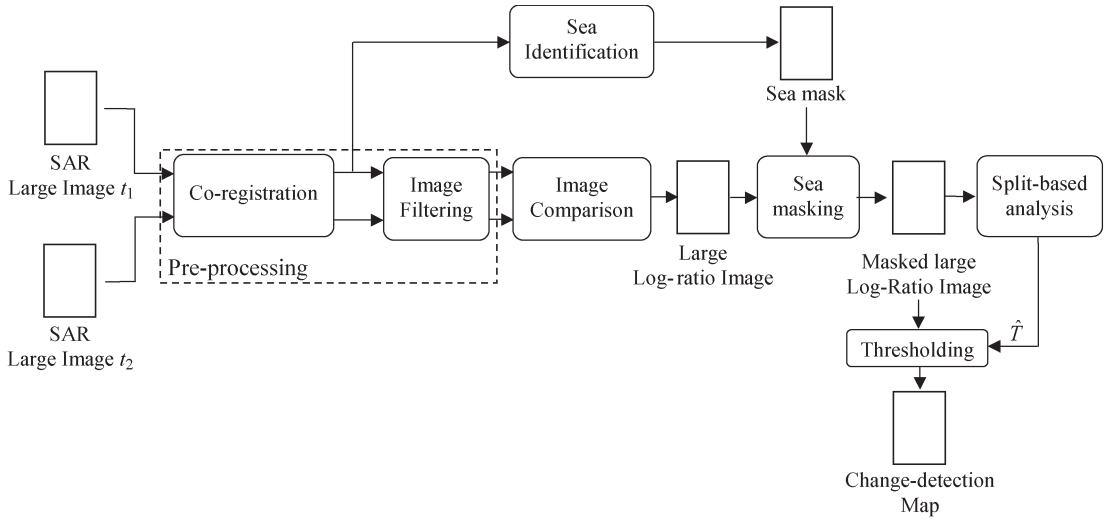

Fig. 3. Block scheme of the proposed system for tsunami-damage assessment.

with the same acquisition parameters, i.e., incidence angle, ascending/descending orbit, and polarization [27].

In order to properly study and characterize the considered problem, a preliminary analysis of the investigated area has been carried out by the following: 1) a visual comparison of high-resolution optical images that were acquired before and after the tsunami and 2) an analysis of the literature. From this analysis, it appears that the tsunami impact varied according to the shape and slope of the ocean floor; the presence or absence of reefs, mangroves, and onshore forests; the orientation and the slope of the coastline; and the underlying rock and soil types. Image analysis shows that some areas have been highly modified by the tsunami. Estuary and wetland sites have apparently been scoured out, and drainage patterns have been changed. Other sites show evidence of subsidence or drainage changes, leading to potential new wetland areas [28]. As stated in [27], with the considered SAR images, it is possible to map eroded coasts, reefs, and foreshores that have become exposed, areas where vegetation has disappeared or has been severely damaged, destroyed piers, quaysides and embankments, and instantaneous extend of inundated areas.

In accordance with the preliminary analysis, in this paper, we decided to investigate the change-detection problem according to two different objectives: 1) to identify only changes that are associated with deep modifications of the environment (such as coast erosion, beach removal, estuary destruction, and areas still flooded at acquisition date after tsunami; we refer to these damages as changes of level 1) and 2) to identify, in a separate way, changes of level 1 and changes that are associated to less severe modification of the environment (such as areas in which vegetation was swept away and buildings were destroyed; we refer to these damages as changes of level 2).

B. Proposed System for Tsunami-Damage Assessment

The architecture of the proposed system (see Fig. 3) is made up of three main parts: 1) image preprocessing and comparison; 2) sea identification and masking; and 3) generation of the change-detection map according to the proposed adaptive SBA.

First, the multitemporal images should be registered in order to obtain alignment between pixels corresponding to the same area on the ground. This process was carried out according to a standard coregistration algorithm for SAR images, which is based on the maximization of cross correlation between images in a given number of selected windows. After coregistration, the part that is common to both the acquisitions is selected to define a multitemporal pair of images having a size of 8662×8192 pixels. Observe that we are clearly in presence of a large-size pair of SAR images.

Due to the active and coherent nature of the SAR signal, both intensity images are affected by multiplicative speckle noise, which may degrade the performances of change-detection techniques. In order to reduce noisy speckle components in the considered images, while preserving sufficient spatial details, adaptive despeckling filters can be used. Many filtering techniques have been published in the literature (e.g., the Frost [29], Lee [30], Kuan [31], and Gamma Map [32], [33] techniques). These filters can be applied with different window sizes (or iteratively) in order to obtain the desired tradeoff between the signal-to-noise ratio and detail preservation.

After preprocessing, the multitemporal images are compared pixel by pixel by means of a log-ratio operator [9], [15].

As expected, according to the considered application, both multitemporal images include large portions of sea. The log-ratio image on the sea has an undesirable behavior that depends on the variability of the conditions during the two acquisition dates (e.g., different weather conditions and presence or absence of waves), which strongly affect the values of the backscattering coefficient. This instability may induce many false alarms. It is worth noting that the use of the difference operator instead of the log-ratio operator could reduce the component to the instability in the sea area due to the small values of the backscattering coefficient. Nevertheless, it has been demonstrated theoretically and experimentally [9]–[13] that the log-ratio operator results in both better statistical properties of the changed and unchanged pixels and in more accurate change-detection maps. In order to solve this problem, in the proposed system, we introduce a block that is aimed at

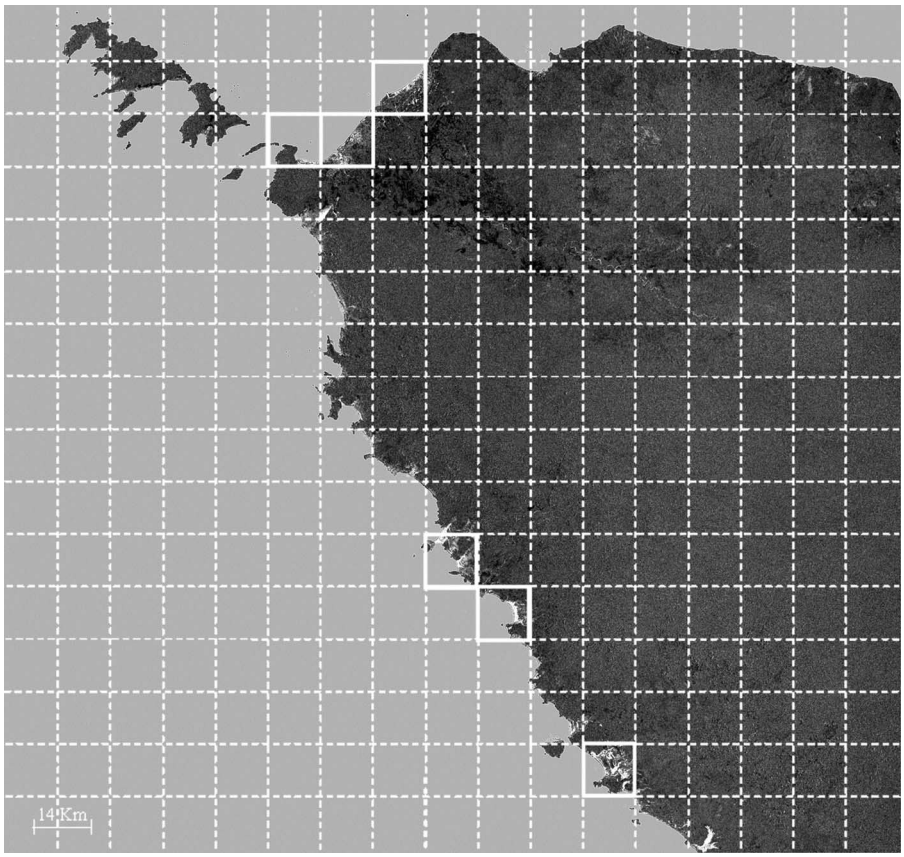

Fig. 4. Log-ratio image after sea masking. The squares that are outlined by white dashed lines identify all the computed splits, while those that are outlined by white continuous lines are the six splits with the highest probabilities of containing changed pixels (in the grayscale black corresponds to the minimum of the log-ratio image, whereas white corresponds to the maximum).

sea identification. A simple automatic unsupervised approach is adopted for detecting sea pixels and filtering them from the change-detection process. Sea or coastline detection in SAR images is a widely investigated topic in the literature [34]–[36]. As we are interested in removing the seaside from the change-detection process, we focus the attention on sea identification rather than coastline detection. In [35], a simple approach is proposed for supervised seaside identification, which is based on two steps: 1) texture feature extraction and 2) supervised classification. The method is based on the observation that the coherent nature of the SAR signal makes the behavior of the texture, due to the speckle on the sea, strongly different from that of the texture on land. In particular, the sea shows a more homogeneous speckle texture than land areas [35] (which are characterized by the presence of various types of land covers) [34]. We propose a similar yet unsupervised approach. As in [35], a texture measure is computed based on the analysis of the cooccurrence matrix; then, an automatic thresholding algorithm is used for separating the sea from the land. Here, the KI thresholding technique that is proposed in [9] has been adopted, which is based on the minimization of a biased estimation of the error probability, under the assumption that the histogram can be modeled according to a mixture of two generalized Gaussian distributions. The described procedure is applied to the image that is acquired before the tsunami in order to produce a conservative sea map and to allow proper identification of the coast erosion due to the tsunami. For taking into account the effects of the window size that is used for computing the texture feature, a margin between the computed mask and the adopted one was imposed. This is not critical because the behavior of the sea along the coast is stable and does not affect the log-ratio image.

Once the log-ratio image has been masked (Fig. 4), it is analyzed according to the SBA that is proposed in Section III. Concerning the threshold-selection algorithm, we also adopted in this step the KI technique that is extended to the generalized Gaussian model that is proposed in [10]. This choice has been done because this algorithm proved to be accurate on change detection in intensity SAR images [10] and, unlike other algorithms that are presented in the literature, it can automatically detect single or double threshold values and can also identify situations in which there are no changes in the analyzed images [10].

IV. Experimental Result

In this section, experimental results that are obtained on the Sumatra Island data set that is presented in Section III-A are shown and analyzed.

A. Design of Experiments

In order to reduce speckle noise components, we applied different despeckling filters (i.e., refined Lee, Frost, and Gamma

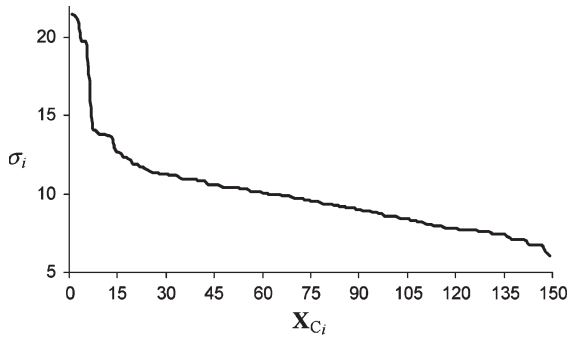

Fig. 5. Diagram of the standard-deviation values σ_i of the considered N splits $\mathbf{X}_{C_i} \in \mathcal{P}_C$ sorted in descending order.

Map) to the considered images. We obtained the best results with the Gamma Map filter. Fig. 4 shows the log-ratio image that is obtained by comparing the two intensity images that are filtered with a Gamma Map filter (the window size is 5×5, with three iterations).[5] This image has been used for all the experiments that are described in this section.

As expected, after comparison, the seaside is strongly unstable due to the high variability of backscattering coefficient in extended water surfaces. Thus, the image that was acquired in April 1998 was analyzed for extracting the mask of sea pixels. In this particular case, we thresholded the entropy measure that was computed from the cooccurrence matrix (the size of the moving window is 7×7 pixels, with interpixel distance 1 in the 45° direction) after requantization on 32 levels. After removing sea pixels from the log-ratio image, unmasked pixels were quantized to integers in the range of [0, 255]. Fig. 4 shows the log-ratio image with masked sea pixels (which are shown in dark gray). This full image was subdivided into 272 splits, each having a size of 509×512 pixels (see dashed lines in Fig. 4). Among them, 123 splits were considered to be unreliable from a statistical point of view, as they include more than 85% of masked pixels (i.e., sea pixels), and thus were removed from the split-based threshold-selection process. The remaining 149 subimages were further analyzed to identify splits with the highest probability to contain changed pixels (see Section II-B). Fig. 5 shows the behavior of the standard-deviation values of the considered subimages sorted in descending order. It is possible to see that, between the first six subimages and all the others, there is a significant difference in the standard-deviation values. Thus, these subimages (see Fig. 6) were selected to perform threshold selection. As expected, all the selected subimages are located along the coast (see splits pointed out with white squares in Fig. 4), where the highest amount of changes occurred. It is worth noting that a preliminary visual analysis of the histogram of the log-ratio image (and of a subset of splits) points out that, on the one hand, the classes of no change and change of level 1 are associated with two modes that are reasonably well separated; on the other hand, the mode of the change of level 2 is strongly overlapped to the other two distributions.

[5]The optimal window size and the number of iterations of the filter were selected according to the procedure that is presented in [13].

Different trials were carried out to assess quantitatively and qualitatively the effectiveness of the proposed system. Two different setups were considered according to the objectives that are described in Section III-A. The two sets of experiments are treated separately in order to properly point out the effectiveness of the proposed system to problems with different complexities.

For both experimental setups, the results that are obtained with the proposed split-based change-detection approach are compared with those that are obtained by applying: 1) the automatic thresholding algorithm to the whole large-size log-ratio image; 2) the automatic thresholding algorithm to each split independently; and 3) the optimal Manual Trial-and-Error thresholding Procedure (MTEP) to each split.[6] The proposed SBA may lead to a noninteger threshold value. In the following, as values in the log-ratio image for simplicity are quantized with integers in the range of [0, 255], all identified threshold values are approximated with the nearest integer.

In order to perform quantitative accuracy assessment, two test sites were selected among the 149 splits having less than 85% of sea pixels. The two test sites were accurately identified for modeling regions of the image with different properties: 1) Split "A" shows a high prior probability of changed pixels. 2) Split "B" shows a small prior probability of changed pixels. According to the properties that are required for split A, it is one of the subimages that are also used for threshold selection (i.e., $\mathbf{X}_{C_5}$). However, we expect that this does not introduce a significant bias in the validation procedure.

For both subimages, a reference map was defined manually according to an accurate visual inspection of both the considered SAR images and a pair of very high geometrical resolution images that are available for the study area. The reference map of split A contains 98 487 unchanged pixels, 14 802 pixels that are associated with the change of level 1, and 20 826 pixels that are associated with the change of level 2. The reference map for split B contains 82 958 unchanged pixels, 1043 pixels that are associated with the change of level 1, and 1554 pixels that are associated with the change of level 2. Figs. 7 and 8 show the log-ratio images and the reference maps (where changes of level 1 are depicted in dark color and changes of level 2 are shown in light gray) of splits A and B, respectively. In all experiments, our goal is to obtain a change-detection map as similar as possible to the reference maps that are yielded according to the aforementioned time-consuming manual process.

B. Change-Detection Results: Single-Change Identification

The first set of trials is aimed at identifying only the change of level 1. In this setup, we neglect the presence of the class of changes of level 2. This assumption does significantly affect the reliability of the thresholding algorithm, which can be applied with a reasonable approximation as the distribution of changes of level 2 is strongly overlapped to others.

[6]The MTEP identifies the threshold by analyzing all possible threshold values and selecting the one resulting in the minimum overall change-detection error compared to the reference map.

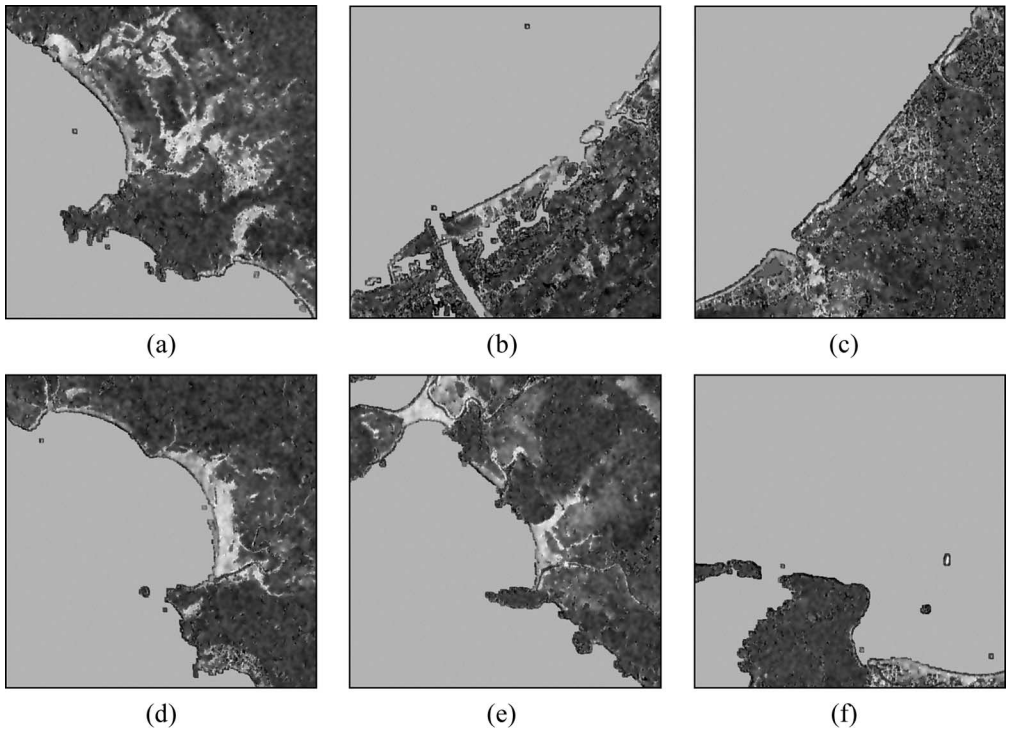

Fig. 6. Masked log-ratio images of the six splits with the highest standard deviation selected according to the proposed split-based change-detection procedure. (a) $\mathbf{X}_{C_1}$; (b) $\mathbf{X}_{C_2}$; (c) $\mathbf{X}_{C_3}$; (d) $\mathbf{X}_{C_4}$; (e) $\mathbf{X}_{C_5}$; (f) $\mathbf{X}_{C_6}$.

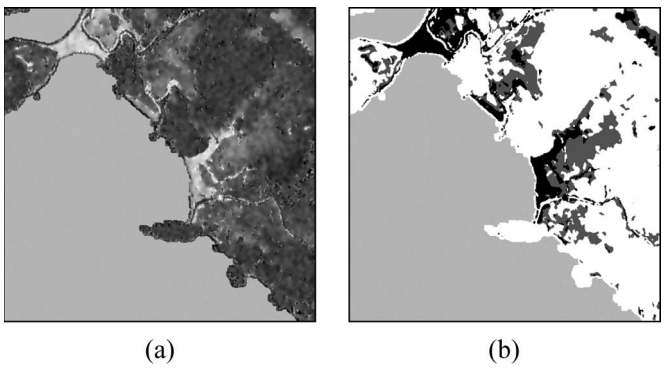

Fig. 7. Test-site associated with split "A" (sea pixels are masked). (a) Log-ratio image, and (b) reference map (the narrow strip of unchanged pixels between the area of change and the sea mask is due to the unchanged sea pixels in the margin).

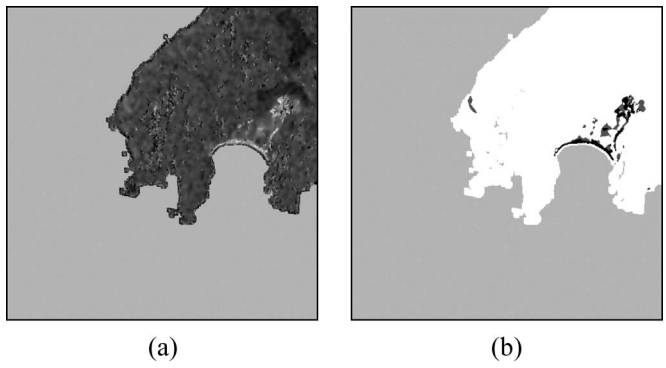

Fig. 8. Test-site associated with split "B" (sea pixels are masked). (a) Log-ratio image, and (b) reference map (the narrow strip of unchanged pixels between the area of change and the sea mask is due to the unchanged sea pixels in the margin).

Table I shows the threshold values that are obtained by applying the KI algorithm independently to the considered splits. As one can see, due to the nonstationarity of the statistical properties of the classes of interest in the spatial domain of the image and to different approximations of the thresholding algorithm in different splits, slightly different threshold values (in the range of 147–166) were obtained.

The results that were obtained on each split were used for computing the final threshold value with the proposed Med-SBA and Mean-SBA strategies. As shown in Table II, both strategies resulted in a threshold value (i.e., 155) that is close to the optimal threshold that was obtained manually (153 for split A and 157 for split B). Thus, the overall error on split A (i.e., 3459) and B (i.e., 553) for both the Med-SBA and the Mean-SBA shows small differences with the overall error that is obtained by the MTEP on the two splits, respectively. The results that are obtained with the J-SBA are slightly better than those that were obtained with the Med-SBA and the Mean-SBA on both splits, as the threshold value (i.e., 154) is closer to the optimal one (i.e., 153).

From Table II, it can also be concluded that all the proposed SBAs performed better than the change-detection analysis that is applied separately to splits A and B. In greater detail, one can observe that, on split A, despite the relative high ratio between

TABLE I
THRESHOLD VALUES FOR THE SIX SPLITS HAVING THE HIGHEST PROBABILITIES TO CONTAIN CHANGED PIXELS (SINGLE-THRESHOLD EXPERIMENT)

Considered split $\mathbf{X}_{C_i}$	$\mathbf{X}_{C_1}$	$\mathbf{X}_{C_2}$	$\mathbf{X}_{C_3}$	$\mathbf{X}_{C_4}$	$\mathbf{X}_{C_5}$	$\mathbf{X}_{C_6}$
Threshold value T_i	150	156	166	153	160	147

TABLE II
THRESHOLD VALUES $\hat{T}$, FALSE ALARMS, MISSED ALARMS, AND OVERALL ERRORS THAT ARE OBTAINED WITH THE SPLIT-BASED APPROACH AND THE THREE PROPOSED COMBINATION STRATEGIES; THE THRESHOLDING ALGORITHM THAT IS APPLIED TO THE WHOLE IMAGE; THE THRESHOLDING ALGORITHM THAT IS APPLIED TO SPLITS "A" AND "B"; AND THE OPTIMAL MANUAL TRIAL-AND-ERROR PROCEDURE

	Threshold-selection technique	$\hat{T}$	False alarms	Missed alarms	Overall errors
Split "A"	Med-SBA	155	1032	2427	3459
	Mean-SBA	155	1032	2427	3459
	J-SBA	154	1259	2109	3368
	Large-size image thresholding	166	158	5750	5908
	Split "A" thresholding	160	397	3974	4371
	MTEP	153	1535	1821	3356
Split "B"	Med-SBA	155	321	232	553
	Mean-SBA	155	321	232	553
	J-SBA	154	362	187	549
	Large-size image thresholding	166	64	608	672
	Split "B" thresholding	-	-	-	-
	MTEP	157	240	301	541

the prior probability of the change and no-change classes, the computed threshold value (i.e., 160) resulted in a higher overall error (i.e., 4371) than the proposed approach. The situation is more critical when considering split B. Depending on the very small ratio between the prior probability of the classes of changed and unchanged pixels, in this split, the threshold-selection algorithm did not identify any threshold value (it recognized a situation where there are no changes).

The proposed SBA also performed better than a direct analysis of the whole large-size log-ratio image, which produces the worst results, due to the small prior probability of changed pixels with respect to the unchanged ones. It is worth noting that, in other experiments (not reported in this paper for space constraints) with different despeckling filters that are applied for the preprocessing of original images, the procedure of threshold selection that is applied to the whole image was not able to identify any decision threshold, while the proposed approach still provided satisfactory results.

Aside from the numerical evaluation that is carried out on the selected test sites (splits A and B), qualitative evaluation of the change-detection maps that were obtained on both splits with the proposed system was also performed (see Figs. 9 and 10). Furthermore, a qualitative analysis of the global change-detection map that was obtained with the SBA was performed (this map is not reported as too large). Both analyses confirmed the effectiveness of the proposed SBA, which produced satisfactory change-detection maps. In order to completely exploit prior information that is available on this specific application, the global change-detection map can be obtained by applying thresholding only to splits along the coast (i.e., splits that contain sea pixels), as, in tsunami-damage assessment, we expect that changes are concentrated only along the coast.

The aforementioned quantitative and qualitative results prove the effectiveness of the proposed approach and its validity at an operational level for the automatic detection of changes of level 1.

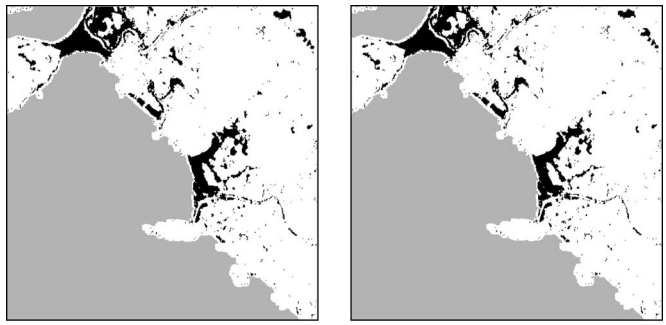

Fig. 9. Change-detection maps obtained on split "A" with (a) the MTEP and (b) the proposed J-SBA (the narrow strip of unchanged pixels between the area of change and the sea mask is due to the unchanged sea pixels in the margin).

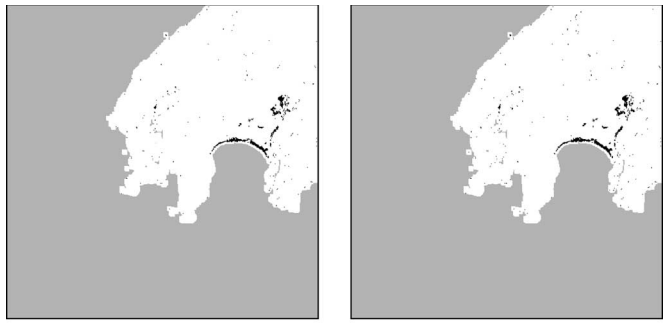

Fig. 10. Change-detection maps obtained on split "B" with (a) the MTEP and (b) the proposed Mean- or Med-SBA (the narrow strip of unchanged pixels between the area of change and the sea mask is due to the unchanged sea pixels in the margin).

C. Change-Detection Results: Double-Change Identification

The second experimental setup is aimed at assessing the effectiveness of the proposed approach in identifying both changes of level 1 and level 2. The detection of changes of level 2 is much more difficult than only the detection of changes of level 1 because of two conditions: 1) The statistical distribution of the related class is highly overlapped to that of the class of no change and partially overlapped to that of the class of change of level 1 (see Fig. 11). 2) Not all the splits in the image (also among the six subimages that are selected for deriving the threshold value according to the proposed SBA) include areas that are associated to change of level 2. This makes much more critical the task of the automatic threshold-selection algorithm, which in the case of double-threshold selection, is intrinsically less robust than in the case of single-threshold selection. This last consideration is confirmed from the results that are reported in Table III, which show the values of the two thresholds that are detected for the six selected splits. As one can observe, the KI algorithm can identify the presence of two threshold values (and, therefore, of two kinds of changes) only in three splits, while for the remaining subimages, only one threshold value is detected. It follows that the proposed combination strategies for estimating the final threshold values were applied to: 1) all the six selected splits when estimating the threshold value that is associated with changes of level 1 $(T_{1,i})$ and 2) only the three

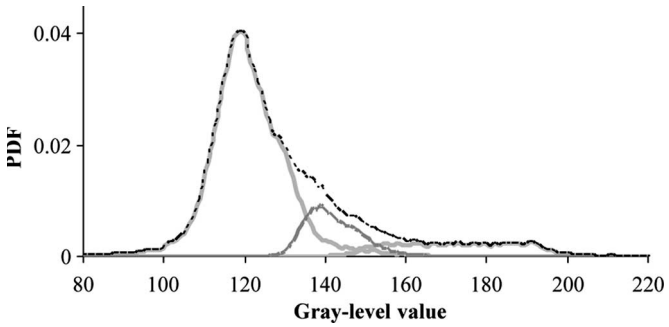

Fig. 11. Probability density function (PDF) of split "A" (black dashed line); and distributions of classes of no-change (light gray line on the left side), change of level 1 (dark gray distribution in the middle) and change of level 2 (light gray line on the right side) evaluated according to the reference map.

TABLE III
THRESHOLD VALUES FOR THE SIX SPLITS HAVING THE HIGHEST PROBABILITIES TO CONTAIN CHANGED PIXELS (DOUBLE-THRESHOLD EXPERIMENT)

Considered split $\mathbf{X}_{C_i}$	$\mathbf{X}_{C_1}$	$\mathbf{X}_{C_2}$	$\mathbf{X}_{C_3}$	$\mathbf{X}_{C_4}$	$\mathbf{X}_{C_5}$	$\mathbf{X}_{C_6}$
Threshold value $T_{i,1}$	150	156	166	153	160	147
Threshold value $T_{i,2}$	127	-	-	136	138	-

TABLE IV
THRESHOLD VALUES $\hat{T}_1$ AND $\hat{T}_2$ AND OVERALL ERRORS THAT ARE OBTAINED WITH THE PROPOSED SPLIT-BASED APPROACH; THE THRESHOLDING ALGORITHM THAT IS APPLIED TO THE WHOLE IMAGE; THE THRESHOLDING ALGORITHM THAT IS APPLIED TO SPLITS "A" AND "B"; AND THE OPTIMAL MANUAL TRIAL-AND-ERROR PROCEDURE

	Threshold-selection technique	$\hat{T}_1$	$\hat{T}_2$	Overall errors
Split "A"	Med-SBA	155	133	10846
	Mean-SBA	155	136	12054
	J-SBA	154	131	12737
	Large-size image thresholding	166	-	-
	Split "A" thresholding	160	138	15245
	MTEP	152	133	10631
Split "B"	Med-SBA	155	133	3832
	Mean-SBA	155	136	3012
	J-SBA	154	131	4808
	Large-size image thresholding	166	-	-
	Split "B" thresholding	-	-	-
	MTEP	151	136	2938

splits when estimating the threshold value separating changes of level 2 $(T_{2,i})$.

As shown in Table IV, all the three proposed SBAs are able to properly identify the two threshold values, which are very close to the threshold values that are obtained with the optimal MTEP for both splits A and B. In particular, for split A, the lowest overall error was obtained with the Med-SBA, which resulted in 10 846 errors with threshold values of 155 and 133. These values are the closest one (among those that were derived by the proposed combination strategies) to the optimal result that was obtained with the MTEP, which identified the pair of threshold values 152 and 133, involving 10 631 errors. Considering split B, the best results were achieved with the Mean-SBA, which identified threshold values 155 and 136, resulting in 3012 overall errors. This error is very close to the one that was yielded by the MTEP (see Table IV).

Since we have three classes, a more detailed analysis of results can be performed by considering the confusion matrices. Here, for space constraints, only the confusion matrices that are associated with the change-detection maps that are obtained with the MTEP for both splits A and B and with the Med-SBA for split A and the Mean-SBA for split B are reported (see Tables V and VI). All the other confusion matrices show a similar trend. By analyzing Tables V and VI, one can observe that, for both splits, the highest number of errors is associated with the class of changes of level 2, which is significantly confused with the other classes. This behavior was expected on the basis of the complexity of the problem as information on the changes of level 2 that are present in the original SAR images is intrinsically ambiguous. However, these results are common to both the proposed SBA and the optimal MTEP; therefore, we can conclude that, in the second setup, the proposed approach also produced satisfactory results.

In addition, in this case, all the proposed SBAs performed better than analysis of either the whole large-size log-ratio image or the single splits A and B independently. In greater detail, as expected, the small prior probability of the change of level 2 and the overlapping between its distribution and those of the other classes resulted in the impossibility of detecting the value of $\hat{T}_2$ by applying the threshold-selection algorithm to the whole large-size log-ratio image. Concerning the change-detection analysis performed independently on split A, the obtained error is significantly higher than the overall errors that were obtained with the proposed approach. Independent threshold selection performed on split B completely failed to identify any threshold value, while the proposed Med-SBA, Mean-SBA, and J-SBA resulted in threshold values that are close to the optimal ones.

In addition, for this setup, a qualitative evaluation of the change-detection maps that were obtained with the proposed system on splits A and B (see Figs. 12 and 13) and on the whole large-size image was carried out. This assessment confirmed the effectiveness of the proposed approach, which despite the complexity of the change-detection problem associated with changes of level 2, produced good-quality change-detection maps. In addition, in this case, we exploited the available prior information in the change-detection process, i.e., we applied the proposed approach only to splits that are along the coast.

V. CONCLUSION

In this paper, an unsupervised and automatic approach for change detection in large-size multitemporal images has been proposed. The proposed approach automatically splits the considered difference (or ratio) image in a set of subimages (splits) of user-defined size, which are sorted out according to their probability to contain a significant amount of changed pixels. The subimages that have the highest probabilities to contain changed pixels are analyzed in order to derive the decision threshold for generating the change-detection map. To this purpose, two different techniques have been proposed: 1) an independent split analysis strategy and 2) a joint split analysis strategy. On the one hand, the joint split analysis strategy has the advantage of jointly modeling the distributions of changed

TABLE V
CONFUSION MATRICES FOR THE CHANGE-DETECTION MAPS THAT ARE OBTAINED ON SPLIT "A" WITH (a) THE PAIR OF THRESHOLD VALUES THAT ARE DERIVED USING THE MTEP PROCEDURE AND (b) THE PAIR OF THRESHOLD VALUES THAT ARE OBTAINED WITH THE PROPOSED MED-SBA

		True Class		
		No-change	Change level 1	Change level 2
Estimated Class	No-change	92729	41	1902
	Change level 1	434	13270	1439
	Change level 2	5324	1491	17485

(a)

		True Class		
		No-change	Change level 1	Change level 2
Estimated Class	No-change	92729	41	1902
	Change level 1	273	12375	759
	Change level 2	5485	2386	18165

(b)

TABLE VI
CONFUSION MATRICES FOR THE CHANGE-DETECTION MAPS THAT ARE OBTAINED ON SPLIT "B" WITH (a) THE PAIR OF THRESHOLD VALUES THAT ARE DERIVED USING THE MTEP PROCEDURE AND (b) THE PAIR OF THRESHOLD VALUES THAT ARE OBTAINED WITH THE PROPOSED MEAN-SBA

		True Class		
		No-change	Change level 1	Change level 2
Estimated Class	No-change	80614	16	357
	Change level 1	429	933	127
	Change level 2	1915	94	1070

(a)

		True Class		
		No-change	Change level 1	Change level 2
Estimated Class	No-change	80614	16	357
	Change level 1	242	811	79
	Change level 2	2102	216	1118

(b)

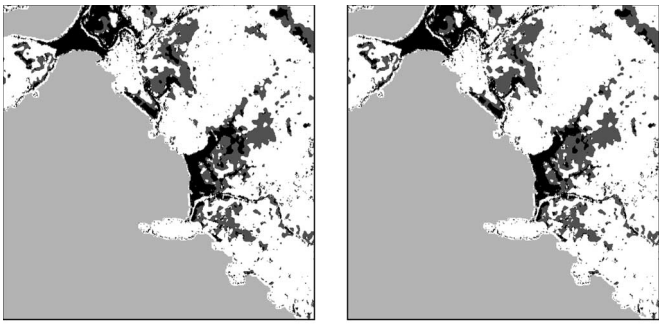

(a) (b)

Fig. 12. Change-detection maps obtained on split "A" with (a) the MTEP and (b) the proposed Med-SBA (the narrow strip of unchanged pixels between the area of change and the sea mask is due to the unchanged sea pixels in the margin).

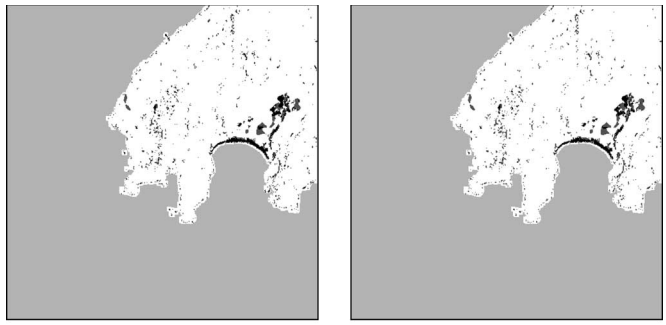

(a) (b)

Fig. 13. Change-detection maps obtained on split "B" with (a) the MTEP and (b) the proposed Mean-SBA (the narrow strip of unchanged pixels between the area of change and the sea mask is due to the unchanged sea pixels in the margin).

and unchanged classes by considering different portions of the images. On the other hand, it has the disadvantage that if, the distributions of classes are slightly different in different splits that are extracted from the large-size image (i.e., the distributions are nonstationary in the scene), the decision threshold that was derived according to model-based thresholding approaches may not be accurate (due to a poor fitting of the joint distribution of classes to the model that is adopted for threshold selection). The independent split analysis strategy overcomes this disadvantage by properly applying the thresholding algorithm separately to each split. It is worth noting that possible nonstationarity in the class distributions results in different values of the thresholds (and thus also affects the results that are provided by the independent split analysis strategy). However, this does not invalidate the models that are adopted for identifying the threshold values but involves the need to fuse the results that are obtained on different splits.

The proposed approach has been used to design a system for damage assessment in relation to the tsunami that occurred in December 2004 in Indonesia. To this purpose, proper architecture that exploits the split-based change-detection system has been defined. Experimental results confirmed the effectiveness of the proposed approach, which detected in an automatic way the main damaged areas. In greater detail, all the three proposed change-detection strategies (i.e., the Mean-SBA, the Med-SBA, and the J-SBA) identified in an automatic way the threshold values for the detection of both changes of levels 1 and 2 that are very close to the optimal values that can be obtained manually. In addition, these strategies revealed to be significantly more accurate and robust than the approaches based on both the independent analysis of each split and the direct analysis of the whole large-size image.

The detection of changes of level 1 is easier due to the good separability between the distribution of such class and that of the no-change class, whereas the strong overlapping between the distribution of the class of changes of level 2 and that of the unchanged pixels makes the identification of such kind of damages less reliable and accurate.

The experimental analysis pointed out that the proposed method requires a computational time that is comparable or smaller than traditional thresholding techniques. This is due to the fact that we split the analysis in subimages, but the additional time that is introduced by the proposed method (split and combination) is negligible with respect to the reduction of the time that we obtain by focusing the threshold-selection algorithm only on a reduced number of pixels (those in the high-standard-deviation splits) instead of on all the pixels of the large-size image.

As a final remark, it is important to observe that, although the proposed SBA has been used to design a system for the detection of damages that are caused by a tsunami by using multitemporal SAR images, potentially, it is general and can be considered for change detection in any pair of large-size multitemporal images. For this reason, as future developments of this work, we plan to extend the experimental investigation to other data sets and change-detection problems to better assess the robustness of the approach in different scenarios.

ACKNOWLEDGMENT

This work has been carried out in the framework of a scientific collaboration with the Joint Research Center of the European Commission [Ispra (VA), Italy]. The authors would like to thank D. Erlich, A. Baraldi, and H. Greidanus for providing the RADARSAT-1 SAR image of Indonesia and for useful discussion on the developed system, and Sarmap s.a. for providing the SARscape software used for image coregistration.

REFERENCES

[1] W. J. Mcguire, B. McGuire, I. Mason, and C. Kilburn, *Natural Hazards and Environmental Change: Key Issues in Environmental Change*. New York: Oxford Univ. Press US, 2002.

[2] A. Singh, "Digital change detection techniques using remotely-sensed data," *Int. J. Remote Sens.*, vol. 10, no. 6, pp. 989–1003, 1989.

[3] P. R. Coppin, I. Jonckheere, and K. Nachaerts, "Digital change detection in ecosystem monitoring: A review," *Int. J. Remote Sens.*, vol. 25, no. 9, pp. 1565–1596, May 2004.

[4] D. Lu, P. Mausel, E. Brondízio, and E. Moran, "Change detection techniques," *Int. J. Remote Sens.*, vol. 25, no. 12, pp. 2365–2407, Jun. 2004.

[5] L. Bruzzone and D. F. Prieto, "An adaptive parcel-based technique for unsupervised change detection," *Int. J. Remote Sens.*, vol. 21, no. 4, pp. 817–822, Mar. 2000.

[6] L. Bruzzone and D. F. Prieto, "A minimum-cost thresholding technique for unsupervised change detection," *Int. J. Remote Sens.*, vol. 21, no. 18, pp. 3539–3544, Dec. 2000.

[7] L. Bruzzone and D. F. Prieto, "Automatic analysis of the difference image for unsupervised change detection," *IEEE Trans. Geosci. Remote Sens.*, vol. 38, no. 3, pp. 1171–1182, May 2000.

[8] L. Bruzzone and D. F. Prieto, "An adaptive semiparametric and context-based approach to unsupervised change detection in multitemporal remote-sensing images," *IEEE Trans. Image Process.*, vol. 11, no. 4, pp. 452–466, Apr. 2002.

[9] Y. Bazi, L. Bruzzone, and F. Melgani, "An unsupervised approach based on the generalized Gaussian model to automatic change detection in multitemporal SAR images," *IEEE Trans. Geosci. Remote Sens.*, vol. 43, no. 4, pp. 874–887, Apr. 2005.

[10] Y. Bazi, L. Bruzzone, and F. Melgani, "Automatic identification of the number and values of decision thresholds in the log-ratio image for change detection in SAR images," *IEEE Geosci. Remote Sens. Lett.*, vol. 3, no. 3, pp. 349–353, Jul. 2006.

[11] R. J. Dekker, "Speckle filtering in satellite SAR change detection imagery," *Int. J. Remote Sens.*, vol. 19, no. 6, pp. 1133–1146, Apr. 1998.

[12] E. J. M. Rignot and J. J. van Zyl, "Change detection techniques for ERS-1 SAR data," *IEEE Trans. Geosci. Remote Sens.*, vol. 31, no. 4, pp. 896–906, Jul. 1993.

[13] C. Oliver and S. Quegan, *Understanding Synthetic Aperture Radar Images*. Norwood, MA: Artech House, 1998.

[14] J. Inglada, "Change detection on SAR images by using a parametric estimation of the Kullback–Leibler divergence," in *Proc. IGARSS*, 2003, vol. 6, pp. 4104–4106.

[15] F. Bovolo and L. Bruzzone, "A detail-preserving scale-driven approach to change detection in multitemporal SAR images," *IEEE Trans. Geosci. Remote Sens.*, vol. 43, no. 12, pp. 2963–2972, Dec. 2005.

[16] R. J. Radke, S. Andra, O. Al-Kofahi, and B. Roysam, "Image change detection algorithms: A systematic survey," *IEEE Trans. Image Process.*, vol. 14, no. 3, pp. 294–307, Mar. 2005.

[17] Y. Bazi, L. Bruzzone, and F. Melgani, "Change detection in multitemporal SAR images based on generalized Gaussian distribution and EM algorithm," in *Proc. Conf. Image and Signal Process. Remote Sens. X, SPIE*, Sep. 13–15, 2004, pp. 364–375.

[18] Y. Bazi, L. Bruzzone, and F. Melgani, "Image thresholding based on the EM algorithm and the generalized Gaussian distribution," *Pattern Recognit.*, 2006, to be published.

[19] P. L. Rosin, "Thresholding for change detection," *Comput. Vis. Image Underst.*, vol. 86, no. 2, pp. 79–95, May 2002.

[20] P. L. Rosin, "Unimodal thresholding," *Pattern Recognit.*, vol. 34, no. 11, pp. 2083–2096, 2001.

[21] P. L. Rosin, "Parcel-based change detection," in *Proc. SPIE Conf. Image and Signal Process. Remote Sens.*, Rome, Italy, 1994, vol. 2315, pp. 289–298.

[22] O. D. Trier and T. Taxt, "Evaluation of binarization methods for document images," *IEEE Trans. Pattern Anal. Mach. Intell.*, vol. 17, no. 3, pp. 312–315, Mar. 1995.

[23] D. Haverkamp and C. Tsatsoulis, "Information fusion for estimation of summer MIZ ice concentration form SAR imagery," *IEEE Trans. Geosci. Remote Sens.*, vol. 37, no. 3, pp. 1278–1294, May 1999.

[24] D. Haverkamp, L. K. Soh, and C. Tsatsoulis, "A dynamic thresholding technique for ice classification," in *Proc. IGARSS*, 1993, pp. 638–640.

[25] N. R. Pal and S. K. Pal, "A review on image segmentation techniques," *Pattern Recognit.*, vol. 26, no. 9, pp. 1277–1294, 1993.

[26] 2005. [Online]. Available: www.disasterscharter.org

[27] H. Greidanus, R. Dekker, J. J. Caliz, and A. Rodrigues, "Tsunami damage assessment with satellite radar," in *Proc. URSI-F Symp. Microw. Remote Sens.*, Ispra, Italy, Apr. 20–21, 2005.

[28] *After the Tsunami: Rapid Environmental Assessment*, 2005. report of the United Nations Environment Programme (UNEP). [Online]. Available: http://www.unep.org/Tsunami/

[29] V. S. Frost, J. A. Stiles, K. S. Shanmugan, and J. C. Holtzman, "A model for radar images and its application to adaptive digital filtering of multiplicative noise," *IEEE Trans. Pattern Anal. Mach. Intell.*, vol. PAMI-4, no. 2, pp. 157–165, Mar. 1982.

[30] J. S. Lee, "Digital image enhancement and noise filtering by use of local statistics," *IEEE Trans. Pattern Anal. Mach. Intell.*, vol. PAMI-2, no. 2, pp. 165–168, Mar. 1980.

[31] D. T. Kuan, A. A. Sawchuk, T. C. Strand, and P. Chavel, "Adaptive noise smoothing filter for images with signal-dependent noise," *IEEE Trans. Pattern Anal. Mach. Intell.*, vol. PAMI-7, no. 2, pp. 165–177, Mar. 1985.

[32] A. Lopes, E. Nerzy, R. Touzi, and H. Laur, "Structure detection and statistical adaptive filtering in SAR images," *Int. J. Remote Sens.*, vol. 41, no. 9, pp. 1735–1758, 1993.

[33] A. Lopes, E. Nerzy, R. Touzi, and H. Laur, "Maximum a posteriori speckle filtering and first order texture models in SAR images," in *Proc. IGARSS*, Collage Park, MD, May 20–24, 1990, vol. 3, pp. 2409–2412.

[34] J. Bijaoui and F. Cauneau, "Separation of sea and land in SAR images using texture classification," in *Proc. IEEE OCEANS*, 1994, vol. 1, pp. 522–526.

[35] A. Niedermeier, E. Romaneeßen, and S. Lehner, "Detection of coastlines in SAR images using wavelet methods," *IEEE Trans. Geosci. Remote Sens.*, vol. 38, no. 5, pp. 2270–2281, Sep. 2000.

[36] J. S. Lee and I. Jurkevich, "Unsupervised coastline detection and tracing in SAR images," *IEEE Trans. Geosci. Remote Sens.*, vol. 28, no. 4, pp. 662–668, Jul. 1990.

Francesca Bovolo (S'05–M'07) received the B.S. (Laurea) and M.S. (Laurea Specialistica) degrees in telecommunication engineering (*summa cum laude*) and the Ph.D. degree in communication and information technologies from the University of Trento, Trento, Italy, in 2001, 2003, and 2006, respectively.

She is currently with the Remote Sensing Laboratory, Department of Information and Communication Technologies, University of Trento. Her research interests include remote-sensing image processing, particularly, change detection in multispectral and SAR images, of which she conducts research within the frameworks of several national and international projects.

Dr. Bovolo is a Referee for the IEEE TRANSACTIONS ON GEOSCIENCE AND REMOTE SENSING, the *International Journal of Remote Sensing*, the *Photogrammetric Engineering and Remote Sensing Journal*, and the *Remote Sensing of Environment Journal*. She served on the Scientific Committee of the SPIE International Conference on "Signal and Image Processing for Remote Sensing XI" (Stockholm, Sweden; September 2006). She is a member of the Scientific Committee of the IEEE Fourth International Workshop on the Analysis of Multi-Temporal Remote Sensing Images (MultiTemp 2007) (Leuven, Belgium; July 2007) and the IEEE International Geoscience and Remote Sensing Symposium 2007 (IGARSS'07) (Barcelona, Spain; July 2007). She ranked first place in the Student Prize Paper Competition of the 2006 IEEE International Geoscience and Remote Sensing Symposium (Denver, CO; August 2006).

Lorenzo Bruzzone (S'95–M'98–SM'03) received the M.S. (Laurea) degree in electronic engineering (*summa cum laude*) and the Ph.D. degree in telecommunications from the University of Genoa, Genoa, Italy, in 1993 and 1998, respectively.

From 1998 to 2000, he was a Postdoctoral Researcher at the University of Genoa. From 2000 to 2001, he was an Assistant Professor at the University of Trento, Trento, Italy, and from 2001 to 2005, was an Associate Professor. Since March 2005, he has been a Full Professor of telecommunications at the University of Trento, where he currently teaches remote sensing, pattern recognition, and electrical communications. He is currently the Head of the Remote Sensing Laboratory in the Department of Information and Communication Technology, University of Trento. His current research interests include remote-sensing image processing and recognition (analysis of multitemporal data, feature selection, classification, regression and estimation, data fusion, and machine learning), of which he conducts and supervises research within the frameworks of several national and international projects. He is Evaluator of project proposals for many different governments (including the European Commission) and scientific organizations. He is the author and coauthor of more than 170 scientific publications, including journals, book chapters, and conference proceedings.

Dr. Bruzzone is a member of the International Association for Pattern Recognition and the Italian Association for Remote Sensing. He is a Referee for many international journals and has served on the scientific committees of several international conferences. He was a Guest Editor of a special issue of the IEEE TRANSACTIONS ON GEOSCIENCE AND REMOTE SENSING on the subject of the analysis of multitemporal remote-sensing images (November 2003). He was also the General Chair and a Cochair of the First and Second IEEE International Workshop on the Analysis of Multi-Temporal Remote-Sensing Images. Since 2003, he has been the Chair of the SPIE Conference on Image and Signal Processing for Remote Sensing. He is also an Associate Editor of the IEEE TRANSACTIONS ON GEOSCIENCE AND REMOTE SENSING and a member of the Scientific Committee of the India-Italy Center for Advanced Research. He ranked first place in the Student Prize Paper Competition of the 1998 IEEE International Geoscience and Remote Sensing Symposium (Seattle, WA; July 1998) and was a recipient of the Recognition of the IEEE TRANSACTIONS ON GEOSCIENCE AND REMOTE SENSING Best Reviewers in 1999.